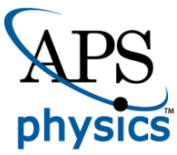

Simple models of the hydrofracture process

M. Marder, Chih-Hung Chen, and T. Patzek

Phys. Rev. E **92**, 062408 — Published 29 December 2015

DOI: 10.1103/PhysRevE.92.062408

Simple Models of the Hydrofracture Process

M. Marder[1], Chih-Hung Chen[1] and T. Patzek[2]
[1]*Department of Physics, The University of Texas at Austin*
[2]*Earth Sciences and Engineering Division, Upstream Petroleum Engineering Research Center, King Abdullah University of Science and Technology*

Hydrofracturing to recover natural gas and oil relies on the creation of a fracture network with pressurized water. We analyze the creation of the network in two ways. First we assemble a collection of analytical estimates for pressure-driven crack motion in simple geometries, including crack speed as a function of length, energy dissipated by fluid viscosity and used to break rock, and the conditions under which a second crack will initiate while a first is running. We develop a pseudo-three-dimensional numerical model that couples fluid motion with solid mechanics and can generate branching crack structures not specified in advance. One of our main conclusions is that the typical spacing between fractures must be on the order of a meter, and this conclusion arises in two separate ways. First it arises from analysis of gas production rates, given the diffusion constants for gas in the rock. Second it arises from the number of fractures that should be generated given the scale of the affected region and the amounts of water pumped into the rock.

I. INTRODUCTION

The extraction of natural gas and oil from mudstones (popularly known as shales) is a technological marvel[1]. The hydrocarbon-bearing layers are thin residues of the floors of ancient bodies of water, now sitting at depths of a kilometer or more. The layers themselves are typically 30 m thick. They are almost completely impermeable, which is why they have managed to hold pressurized natural gas for tens of millions of years. The process of horizontal drilling and hydrofracturing breaks these layers, introducing new fractures and activating old ones, creating a transport network that allows the gas to come to the surface.

The hydrofracture process is incontestably effective. Following a process that includes injection of acid, detonation of casing perforation charges, and injection of pressurized water mixed with sand, gas and oil emerge from the previously impermeable layer[2]. The process was developed empirically, and what exactly happens underground is somewhat mysterious. Micro-seismic measurements provide a very coarse indication of the extent of the fractures, and resistivity logs during the drilling process provide some information about the frequency of natural fractures in the mudstone prior to drilling. The precise geometry of the fracture network is unknown.

Our goal here is to present simple analytical estimates and describe a numerical framework that let us begin to address how the network geometry is created. We have already obtained some hints about the network geometry from a different source of information, the volume of gas arriving over time from the wells[3]. We present one of the main conclusions of the previous work in a somewhat new way so as to emphasize the problem it presents.

Let us suppose that the fractures allowing gas to escape from a hydrofractured well are all straight, parallel and equally spaced with effective spacing d, as shown in Figure 1. Next assume that the permeability k of the region between fractures is uniform and given by laboratory values of uncracked core samples: on the order of a nanodarcy. The fractures are assumed to have such great permeability that once gas reaches them it arrives at the surface immediately.

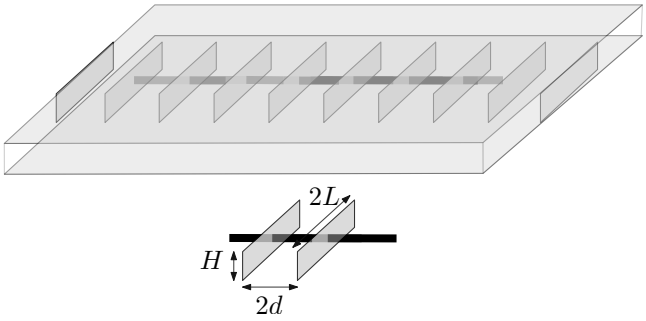

Figure 1: Schematic geometry of horizontal well.

Given these assumptions, and taking k to equal precisely one nanodarcy, one can deduce from the production history of each well the effective spacing d, through the relation from Ref [3] $\tau = d^2/\alpha$, where τ is a time to interference deduced from the production history of each well, and α is the diffusivity of gas in the unbroken matrix: when the permeability is one nanodarcy, the diffusivity is 3×10^{-8} m^2/s.

After computing τ from 2057 wells in the Barnett shale, we assemble the effective spacings d obtained in this way in Figure 2. The effective spacing peaks at about 1.5 m. On its face this seems an unrealistic value. The hydrofracturing process involves creating fractures in 10-20 stages along a horizontal length of around 1500 m. Therefore one would expect a typical spacing of 75-100 m. In addition, it is impossible that a physical process naturally creates a series of identical planar fractures, 30×200 m, spaced by 1.5 m. Therefore, the 1.5 m spacing must be understood as the characteristic scale of geometrical configuration that is considerably more complicated than what is shown in Figure 1, with branches and interconnections. It is more likely to be fractal than uniformly spaced.

Still, what this calculation indicates is that the very low permeability of unbroken segments of shale, combined with the observed rate of production, demand that in the end the gas emerge from a conducting network with spacing on the order of a meter. Whether this network is created purely by the hydrofracturing process, mainly consists of a pre-existing

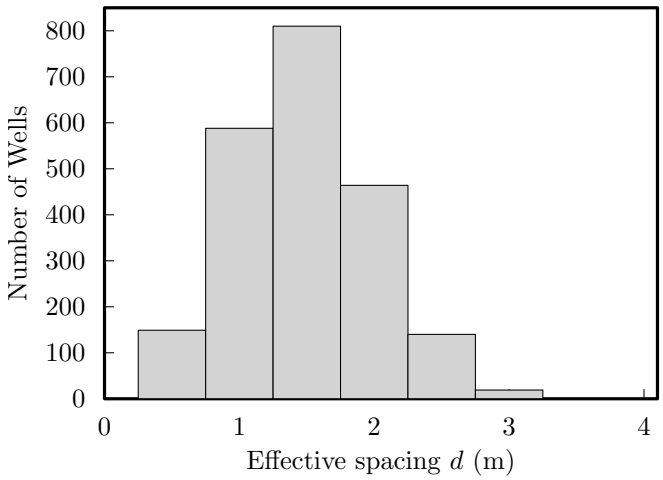

Figure 2: Histogram showing the number of wells with different effective spacings d, estimated from production history in Barnett Shale.

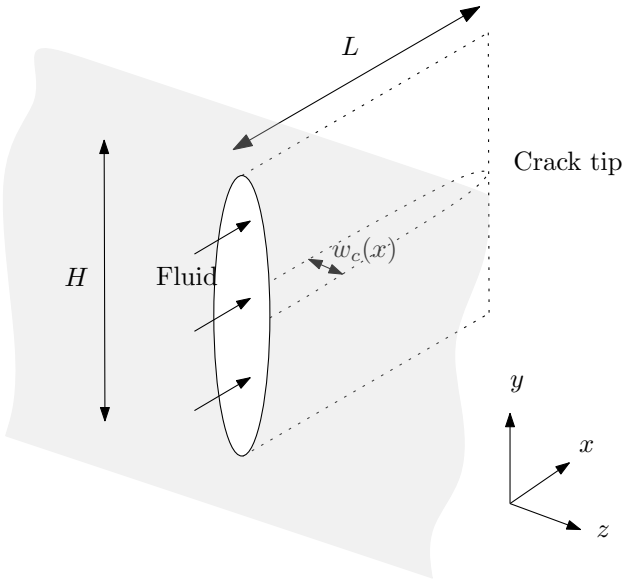

Figure 3: Geometry first employed by Perkins and Kern[4] to study fluid-driven fractures.

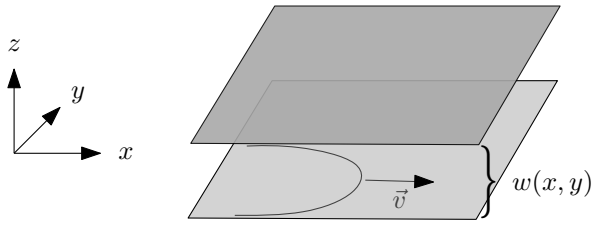

Figure 4: Geometry of lubrication approximation.

network of natural fractures, or some combination of the two is not so important. Accounting for it is the main problem that occupies this paper.

In Section II we review analytical models of pressure-driven cracks and assemble simple analytical relations that describe them.

In Section III we construct a numerical model that allows fluid and breaking rock to interact in a unified way without specifying crack paths in advance.

In Section IV we use the numerical model to examine test cases based on analytical results and to explore factors such as inhomogeneity and external stresses.

In Section V we present concluding remarks.

II. ANALYTICAL EXPRESSION FOR FLUID-DRIVEN CRACKS

Summary of theory for elliptical fluid-driven crack

The creation of cracks underground by injection of water has been studied for a long time. In a classic early article, Perkins and Kern[4] proposed a simple geometrical setting where good approximations are available and analytical progress is possible. As shown in Figure 3, the crack is assumed to be of uniform height H, elliptical cross section, and width $w_c(x)$ along its minor axis. Fluid flows into the opening and causes the crack to extend. Nordgren [5] extended to the model to include the possibility of fluid loss, so this setting is referred to as the PKN model.

Perkins and Kern considered both laminar and turbulent fluid flow in the elliptical crack. More recently, the advance of numerical methods has made it possible to relax many of their simplifying assumptions and solve more realistic problems using finite element methods. This approach to the problem was pioneered by Clifton[6–9]. In this and more recent numerical work [10, 11] it is customary to assume that fluid flow in the crack is laminar, although assumptions such as uniform height H and elliptical cross section are dropped.

Later in this article we will construct a pseudo-three-dimensional model of fluid interacting with and fracturing rock. However it is possible to extract a considerable amount of insight by simplifying the problem to the point where analytical expressions are available.

To begin, we imagine that each half of one of the fracture wings in Figure 1 is a PKN crack of the sort shown in Figure 3. We review the results of Perkins and Kern, simplifying the presentation, adding some results that are useful for the dynamics of fracture, and then ask what one can deduce from a typical hydrofractured horizontal well.

Even in realistic numerical simulations (e.g. [10]) it is customary to adopt the lubrication approximation for fluid flowing into the crack, as shown in Figure 4. In this approximation, the fluid flow has a parabolic profile between two locally parallel walls separated by distance w. In the presence of a pressure gradient $\vec{\nabla} P(x,y)$ the fluid flow takes the approximate form

$$(v_x, v_y, v_z) \approx \vec{u} f(z) + \hat{z} v_z = \vec{u} \frac{z}{w} \left(1 - \frac{z}{w}\right) + \hat{z} v_z. \qquad (1)$$

and the velocity $\vec{u}(x,y)$, which is four times the velocity at the center of the channel, is given by

$$\vec{u} = -\frac{w^2}{2\mu}\vec{\nabla}P. \tag{2}$$

Incompressibility of the fluid then requires that walls move apart at the rate given by v_z. Thus solving for v_z and setting it to $\partial w/\partial t$ gives

$$\frac{\partial w}{\partial t} = \vec{\nabla}\cdot\frac{w^3}{12\mu}\vec{\nabla}P. \tag{3}$$

This expression is standard in numerical studies of hydraulic fracturing. To employ it in the context of the elliptical crack we employ four simplifications. First, we assume that pressure is independent of y: $P = P(x)$. Second, we apply Eq. (3) on the minor axis where the crack has width w_c. Third, we assume that the crack retains its elliptical cross section as it grows. Fourth, and finally, we assume that the flux of water Q into the crack is constant.

The total flux of water Q going through the crack at some point x is given by the x component of $\vec{u}$:

$$Q = \int dy\, w(x,y)u_x(x,y). \tag{4}$$

Carrying out this integral for an elliptical cross section gives

$$Q = -\frac{\pi\left(w_c/2\right)^3(H/2)}{4\mu}\frac{\partial P}{\partial x}. \tag{5}$$

Here w_c is the width of the center of the crack, across the minor axis. This expression agrees with Lamb [12, XI.290, p. 523]. To close the theory, we employ an approximate expression that relates the pressure P on the faces of the crack to the opening width w_c. Let Young's modulus of the surrounding elastic medium be Y. Then a result due to Sneddon gives [4, 13]

$$w_c(x) = \beta P(x) \text{ where } \beta = \left(\frac{Y}{2H(1-\nu^2)}\right)^{-1}. \tag{6}$$

Insert Eq. (6) into (3). Integration gives for pressure and crack width along the minor axis the expressions

$$P(x) = 4\left(\frac{Q\mu(L-x)}{\pi H\beta^3}\right)^{1/4}; \tag{7}$$

$$w_c(x) = 4\left(\beta Q\mu(L-x)/\pi H\right)^{1/4}. \tag{8}$$

The dissipation of fluid flowing through the channel is dominated by the shear flow across z and, using (1), is

$$D/w = \frac{1}{2}\mu\left[\left(\frac{\partial v_x}{\partial z}\right)^2 + \left(\frac{\partial v_y}{\partial z}\right)^2\right]. \tag{9}$$

Integrating over the width of the channel gives $D = u^2\mu/6w$ and the total dissipation due to viscosity of the fluid is

$$\mathscr{D} = \frac{16}{3}\left(\frac{2\mu LQ^5Y^3}{\pi^5(1-\nu^2)^3H^4}\right)^{1/4}. \tag{10}$$

The total volume V occupied by the crack is given by integrating the cross-sectional area over the length. Assuming no water loss, this must equal total injected water volume W giving

$$V = W = \frac{8}{5}\left(\frac{\pi^3\mu\left(1-\nu^2\right)H^4L^5Q}{8Y}\right)^{1/4}. \tag{11}$$

Inverting this relation gives crack length as a function of injected water volume W and flow rate Q:

$$L = \left(\frac{5^4W^4Y}{8^3\pi^3\mu\left(1-\nu^2\right)H^4Q}\right)^{1/5}. \tag{12}$$

From $Q = dV/dt$ (and assuming Q to be constant) one obtains the crack speed

$$\dot{L} = \left(\frac{Q^3Y}{2\pi^3\mu\left(1-\nu^2\right)H^4L}\right)^{1/4}. \tag{13}$$

One can also calculate the mechanical work done on the crack faces, and from this calculation determine the conditions under which crack propagation occurs. The condition for crack propagation is that the total work done on the crack faces when the crack extends by amount dL be greater than or equal to the energy cost of creating the extra surface area, namely $\Gamma H dL$.

The work done on the crack faces by injection of fluid is

$$\begin{aligned} dE &= \int_o^L dx\int_0^H dy\, P(x,y)\frac{dw(x,y)}{dL}dL. \\ &= H\frac{\beta}{3}P^2(x=0)dL. \end{aligned} \tag{14}$$

Thus the condition for crack propagation to be possible is

$$\frac{\beta}{3}P^2(x=0) > \Gamma. \tag{15}$$

Canonical Calculations

We now adopt dimensionless units based on typical field values for all the quantities we have used so far and explore the implications for orders of magnitude in the problem. Table I lists reference values for all the important quantities in the hydrofracturing problem. To obtain dimensionless quantities, scale a variable by its reference value. For example $\tilde{Q} \equiv Q/Q_0$, $\tilde{W} \equiv W/W_0$ and so on. The dimensionless quantities all have a tilde above, while reference values all have the subscript 0.

Dimensionless Group

Consider the limit in which $L \gg H$. The height of the crack H should appear only in the combination Q/H, since the physical conditions are unchanged so long as the water flux Q and the crack height H increase simultaneously by the

Table I: The variables in this paper and their reference (canonical) values, all expressed in SI units.

Variable	Description	Reference Value	Units SI
Q	Water rate into crack per direction	$Q_0 = 0.1325^a$	m^3/s
W	Total volume of injected water per stage^b per direction	$V_0 = 795^c$	m^3
N	Total number of cracks	1	-
L	Length of crack along one direction	$L_0 = 100$	m
H	Height of crack	$H_0 = 30$	m
μ	Fracturing water viscosity	$\mu_0 = 10^{-3}$	Pa s
Y	Rock Young's modulus	$Y_0 = 50 \times 10^9$	Pa
t	Fracture time	$t_0 = 1$	s
ν	Poisson's ratio	.25	-
Γ	Specific fracture energy	$\Gamma_0 = 100$	J/m^2

[a] 50 bbl/minute
[b] Hydrofracture stage that involves 4-5 perforation clusters, each with dozens of perforations, along a well segment 75–150 m long isolated with packers
[c] 5000 bbl

same factor. Since $H/L \approx 0$, it does not appear in expressions for physical quantities. The quantities $Q/H, \mu, Y$, and L can form only one dimensionless factor which is

$$\kappa \equiv \left(\frac{Q\mu}{HYL^2}\right)^{1/4}. \tag{16}$$

The 1/4 power reflects the way this parameter arises if one computes w/L. For the canonical values of Table I, $\kappa = 9.69 \times 10^{-6}$.

It is not easy to preserve this value in a model system. For example, if one takes a material where Young's modulus is 10 GPa, the liquid is water, and the system height $H =$ 0.5 m, then κ is preserved for a flow of $Q = 0.1$ cm^3/s and $L = 1.5$ m. A hundred-fold decrease in Young's modulus for a floppier material such as a gel would need to be compensated by a tenfold increase in L to 15 m.

Pressure at base of crack

We now proceed to provide typical values of various quantities in canonical form, starting with the pressure:

$$P(x=0) = 2.24\left(\frac{\tilde{\mu}\tilde{L}\tilde{Q}\tilde{Y}^3}{\tilde{H}^4}\right)^{1/4} \text{MPa} = 1.10\left(\frac{\tilde{\mu}\tilde{t}\tilde{Q}^2\tilde{Y}^4}{\tilde{H}^6}\right)^{1/5} \text{MPa}. \tag{17}$$

This comes from Eq. (7). Pressure is on the order of mega-Pascal.

Crack width at along semi-major axis at base of crack

$$w_c(x = 0) = 2.52 \times 10^{-3}\left(\frac{\tilde{L}\tilde{Q}\tilde{\mu}}{\tilde{Y}}\right)^{1/4} \text{m} \tag{18}$$

This comes from Eq. (8). The opening at the base of the crack is on the order of millimeters.

Crack length

$$\tilde{L} = 60.1\left(\frac{\tilde{W}^4\tilde{Y}}{\tilde{\mu}\tilde{H}^4\tilde{Q}}\right)^{1/5} \tag{19}$$

$$L = 6006\left(\frac{\tilde{W}^4\tilde{Y}}{\tilde{\mu}\tilde{H}^4\tilde{Q}}\right)^{1/5} \text{m} = 5.70\left(\frac{\tilde{t}^4\tilde{Y}\tilde{Q}^3}{\tilde{\mu}\tilde{H}^4}\right)^{1/5} \text{m}. \tag{20}$$

This results from Eq. (12); the expression involving time makes use of $\tilde{W} = \tilde{Q}\tilde{t}/6000$, which follows from the definitions of the dimensionless flow rate $\tilde{Q}$ and dimensionless water volume $\tilde{W}$.

Dissipation in fluid per unit crack advance (dissipation per time over change in crack areas per time)

$$\mathscr{D}/\dot{L}H = 3770\sqrt{\frac{\tilde{Q}\tilde{L}\tilde{\mu}\tilde{Y}}{\tilde{H}^2}}\,\frac{\text{J}}{\text{m}^2}. \tag{21}$$

This comes from Eq. (10). Dissipation in the fluid is typically ten times the fracture energy of the rock, which is hundreds of Joules per square meter.

Crack speed

$$\dot{L} = 2.22\left(\frac{\tilde{Q}^3\tilde{Y}}{\tilde{H}^4\tilde{L}\tilde{\mu}}\right)^{1/4}\frac{\text{m}}{\text{s}}. \tag{22}$$

This comes from Eq. (13). The typical crack speed is meters per second.

Condition for crack propagation

$$1885\sqrt{\frac{\tilde{\mu}\tilde{L}\tilde{Q}\tilde{Y}}{\tilde{H}^2}}\frac{\mathrm{J}}{\mathrm{m}^2} > \Gamma. \tag{23}$$

This follows from Eq. (15). Since fracture toughness is on the order of 100 J/m^2 this implies that seed cracks can be 400 times smaller than 100 m, or .25 m in length for propagation to start. Note that this is the same dimensionless combination that showed up in Eq. (21) and is half the energy dissipated in the fluid.

Time

How long does it take a crack to reach a given length?

$$t = 35.9\left(\frac{\tilde{\mu}\tilde{L}^5\tilde{H}^4}{\tilde{Q}^3\tilde{Y}}\right)^{1/4}\mathrm{s}. \tag{24}$$

Initiation of Multiple Cracks

Recall that we chose dimensionless variables to correspond to typical values for the hydrofracture of a single stage in a horizontal well. Setting variables on the right hand side of Eq. (19) to one should therefore give a value of order one for the left hand side. This is not the case. Given the total volume of injected water per stage per direction, if one assumes that the result of the fracture process is a single crack, that crack is more than 60 times larger than the known typical extent of the fracture zone around the well. In other words, all the dimensionless quantities have chosen because in practical situations they are of order unity. However inserting 1 for all of them in Eq. (19) gives the equation $1 = 60.1$. Something must be wrong.

One possibility is that a great deal of the water injected into the fracture somehow seeps away and is lost. Such an effect could be incorporated formally into the model by making the non-dimensional total water volume $\tilde{W}$ smaller by a factor of 60 while keeping other quantities fixed. However doing so would violate an important part of our physical picture, which is that except where it is fractured the shale is nearly impermeable to gas and water. Simply positing that most of the water disappears would be incompatible with the picture.

Therefore, we propose that the hydrofracturing process creates the equivalent of 100-200 cracks of length L_0. A question that next arises is how this structure grows. Physical arguments using Eq. (23) lead to the conclusion that cracks mainly grow one at a time. To see why, suppose that at some time there are two seed cracks leading off the well of a length 1 m. According to Eq. (23), the water flow will be enough for one of them to propagate. If however both of them were to start propagating, then the water flux Q would have to be shared between the two of them, it would drop to half the total value, and neither would have sufficient driving force to break the rock and advance. Therefore, one of the cracks can be expected to grow at the expense of the other. As the crack grows, the mechanical energy flux to the crack tip will come to exceed by a larger and larger factor the minimum energy needed to create new crack surfaces. As we know from studies of crack tip instabilities, this energy can be accommodated through the creation of damage on micron scales in the vicinity of the crack tip[14]. However, it is interesting to ask why the single crack would ever stop propagating. One possibility would be that it hits another rock layer of considerably greater toughness. However, as the crack is traveling laterally in the shale, there is no easy way for this to happen, although this mechanism presumably is what limits the cracks to vertical height H. Another possibility is that the single crack tip becomes unstable and splits. This however would not put an eventual limit on the length of the branching cracks. A final possibility is that each crack stops propagating when the energy dissipated within the fluid becomes so great that it is energetically favorable to start another crack instead.

To get a sense of how this might happen, let us consider the process of crack initiation more carefully. Seed cracks will be irregularly shaped, but suppose for simplicity that the seed is of height H but length $L \ll H$. In this case, Eq. (6) is replaced by

$$\beta = \left(\frac{Y}{2L(1-\nu^2)}\right)^{-1}. \tag{25}$$

Consider a short static crack of this sort. Because the crack is static, the pressure inside is constant. The mechanical work involved in a small extension by amount dL is

$$\begin{aligned} dE &= \int_o^L dx \int_0^H dy P\frac{dw(x,y)}{dL}dL \\ &= LHP^2\frac{d\beta}{dL}dL = LP^2H\frac{2\left(1-\nu^2\right)}{Y}dL. \end{aligned} \tag{26}$$

Setting this energy equal to the energy for crack propagation $\Gamma H dL$ gives a standard expression for the critical pressure at which an edge crack begins to propagate:

$$P_c^{\mathrm{static}} = \left(\frac{Y\Gamma}{2L(1-\nu^2)}\right)^{1/2} = 0.16\sqrt{\frac{\tilde{\Gamma}\tilde{Y}}{\tilde{L}}}\mathrm{MPa}\,. \tag{27}$$

We now explore a particular scenario that corresponds to simulations performed below. Suppose there are two seed cracks of nearly but not exactly the same length, say 1 m, which in our dimensionless units is $\tilde{L}$=.01. The longer of them will start to propagate when the pressure reaches a critical value for initiation, as in Eq. (27). For $\tilde{L} \approx .01$, the static pressure Eq. (27) at which the crack initiates is greater than the dynamic pressure Eq. (17) in the crack once it begins to move. In fact our analytical expressions for moving cracks are only accurate when their length L is much greater than their height H, and this condition does not obtain in the first time after the crack starts to run. However the conclusion

that the pressure drops is correct, as one finds from the simulations. Thus pressure falls below the level needed to trigger the second crack, which for the time being will remain static. The first crack continues to run and when it reaches values of $L \gg H$, Eq. (17) can be applied and gives a pressure at the base of the crack that rises as the one quarter power of Q and L. Eventually the pressure at the base of the crack must reach a value sufficient to trigger the second seed crack. In the particular case of the simulations below, we will see that seed cracks of about a meter produce dynamic fractures that get to a length of around $\tilde{L} \approx 1 \Rightarrow L = 100$ m before new fractures are triggered.

Now there are two cracks propagating, with lengths $\tilde{L}_1$ and $\tilde{L}_2$, driven by flows $\tilde{Q}_1$ and $\tilde{Q}_2$ respectively. Conservation of fluid implies that

$$\tilde{Q} = \tilde{Q}_1 + \tilde{Q}_2. \tag{28}$$

Their relative speeds can be determined as follows. Assume that the pressures at the bases of the two cracks are the same. According to Eq. (17), this can only be the case if

$$\frac{\tilde{L}_1}{\tilde{L}_2} = \frac{\tilde{Q}_2}{\tilde{Q}_1}. \tag{29}$$

From Eqs. (22) and (29) the ratio of the growth rates is

$$\frac{\dot{\tilde{L}}_2}{\dot{\tilde{L}}_1} = \left(\frac{\tilde{Q}_2^3 \tilde{L}_1}{\tilde{Q}_1^3 \tilde{L}_2} \right)^{1/4} = \frac{\tilde{L}_1}{\tilde{L}_2}. \tag{30}$$

Therefore the smaller of the two cracks has a greater velocity, in proportion to the ratio of the lengths. This mechanism will eventually lead the lengths of the two cracks to converge.

For more than two cracks the picture becomes increasingly complicated, but the computation makes it plausible that cracks initiate and run, tending to catch up with the previous cracks until the back pressure rises to the point where it triggers yet another crack and the process repeats.

Estimate of numbers of cracks from fracture mechanics

To conclude this section, we return to Eq. (19) and assume that cracks reach a length of 100 m, computing the number of cracks of this sort that would have to form to absorb the injected water, and then computing the spacing between them. More specifically, let there be n cracks per stage per direction each absorbing a part W/n of the water. Then the number of cracks is given by

$$\tilde{L} = 1 = 60.1 \left(\frac{\left(\tilde{W}/n\right)^4 \tilde{Y}}{\tilde{\mu} \tilde{H}^4 \tilde{Q}} \right)^{1/5} \Rightarrow n = \frac{167 \tilde{W} \left(\tilde{Y}/\tilde{\mu}\tilde{Q}\right)^{1/4}}{\tilde{H}}. \tag{31}$$

To explore the implications of these calculations, we acquired data on a number of wells in the Marcellus shale, describing the number of stages, total fluid injected, and lateral length. The data include values for $\tilde{W}$ and $\tilde{Q}$. All other dimensionless physical parameters are set to the nominal value of 1. Solving for n, Table II shows the typical spacing between fractures. This spacing is on the order of 0.5 m, which is consistent with the values in Figure 2, although on the low side. We note that the data in Figure 2 come from the Barnett shale, while the data in Table II come from the Marcellus shale, which should be expected to be similar, but not identical. The comparison of two different formations is explained on the one hand by the difficulty of obtaining data such as those in Table II, and on the other by the fact that our purpose is to illustrate orders of magnitude.

Thus two completely separate lines of analysis converge: physical considerations based on the fracture process and considerations based on the extraction of gas give a consistent account of the effective spacing between fractures.

III. SIMULATION METHOD

Having laid out the expected behavior of cracks under the assumptions of the PKN model, we turn to a numerical method capable of simulating the problem. We adopt an intermediate level of description. We want to treat the mechanics of fracture in greater detail than in a percolation model such as Quinn, Turcotte, and Rundle[15]. On the other hand, given the desire to treat multiple interacting cracks over scales of hundreds of meters, we are forced to include less detail than in customary hydraulic fracture simulations[10]. The design goals for the numerical method are:

1. It will reproduce the behavior of PKN cracks in cases where a single crack runs at a time.
2. The model will be posed in two dimensions, without any necessary constraint on the crack path or number of cracks.
3. Fluid motion, elastic deformation, and crack propagation will all come out of the model based on underlying physics.

To achieve these goals, note that the smallest timescale in the problem is the time needed for fluid pressure to equilibrate locally within a small region of a fracture filled with fluid. As shown above, the characteristic width of a hydraulic fracture is 1 mm. Since the speed of sound in water is 1500 m/s, the characteristic time for pressure equilibration is $10^{-5} - 10^{-7}$ s. By way of contrast, we will be examining lumped elastic models for the rock, where a characteristic spacing within the rock is 1m. Even though the speed of sound in rock is several times greater than in water, the larger spatial scale means that the characteristic time for rock to move during dynamic fracture will be 10^{-3} s. This is not a huge separation of time scales, but treating pressure equilibration across fracture widths as instantaneous appears to be the best starting point. It leads to great gains in numerical efficiency, since taking pressure equilibration of the fluid to be fast means there is no need to model the fluid in detail. We employ the lubrication approximation, Eq. (3).

The geometry of the model is sketched in Figure 5. It contains the following ingredients. First, there is a set of mass

Well Name	*Lateral Length* (ft)	*No. Stages*	*Total Fluid* (bbl)	*Total Sand* (ton)	*Frac Rate* (bpm)	$\tilde{Q}$	$\tilde{W}$	n	d (m)
W1	4709	18	170870	7996	80	0.8	0.95	168	0.48
W2	4046	17	146360	6616	79	0.79	0.86	153	0.48
W3	3921	16	120059	6750	87	0.87	0.75	130	0.50
W4	5709	23	164324	9533	88	0.88	0.71	123	0.61
W5	6055	14	143581	9373	80	0.8	1.03	181	0.73
W6	4534	11	105478	7031	87	0.87	0.96	166	0.76
W7	7674	16	184290	10426	88	0.88	1.15	199	0.74
W8	3566	8	93455	5518	90	0.9	1.17	200	0.68
W9	6168	13	147826	7882	76	0.76	1.14	203	0.71
W10	5017	12	142007	7330	78	0.78	1.18	210	0.61
W11	5773	13	146209	7906	75	0.75	1.12	202	0.67
W12	5891	13	133314	7858	74	0.74	1.03	185	0.75

Table II: Properties of Marcellus wells, expressed in field units: bbl=barrel=.159 m^3; bpm=barrels per minute. Note that the spacing in the final column is comparable to the spacing, deduced by completely different means, in Figure 2, although very much at the lower end.

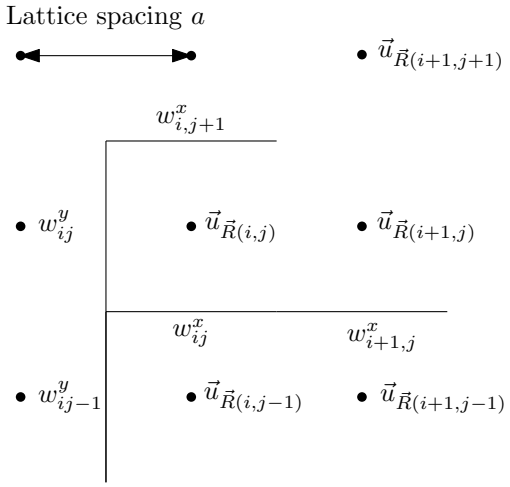

Figure 5: Structure of lattice model of hydrofracture. The lattice spacing is a. Mass points are located at points $u_{\vec{R}}$. When the distance between mass points exceeds a critical value (the increase is small compared to the lattice spacing) bonds break, channels open up between them, and their width is $w^{x,y}_{ij}$. Channels are indicated by solid lines.

points $\vec{u}_{ij}$ arranged on a square lattice. These mass points interact with nearest neighbors only and have a force law that is a general linear functional of relative displacements of neighbors. It is not just a function of distance. Therefore although the points are defined on a square lattice, the lattice can have any desired shear resistance. Second there is a fracture criterion based on separation of mass points. The physical separation of the mass points will be understood to be on the order of a meter, and the fracture criterion will correspond to motions on the order of a small distance $\delta \ll 1$ mm calculated below. Therefore this model will not involve neighbors switching places. Note that this model fully contains two-dimensional linear elasticity plus fracture mechanics. The orders of magnitude are as follows:

Young's modulus for rock is typically 50 GPa. Fracture energy is typically 100 J/m^2. For a spring of length $a = 1$ m the extension at failure is of order $\delta = \sqrt{2\Gamma a/Y}$ which comes out to 6×10^{-5} m. The longitudinal spring constant for the model is $k_\parallel = Ya/(1-\nu^2) \approx 50 \times 10^9$ J/m^2 .

Here is how the model operates. So long as all the bonds on a mass point are unbroken, the mass point evolves in accord with the mechanical forces on it. As soon as a bond breaks between two mass points, a channel w between the two mass points is activated, and the distance between the mass points on either side is now controlled by Eq. (3) rather than elasticity. The pressure $p_{\vec{R}\vec{R}'}$ in any channel segment passing between points $\vec{R}\vec{R}'$ is given by the average normal force of mass points on either side.

The elastic force on mass point $\vec{u}_{\vec{R}}$ is

$$\vec{F}_{\vec{R}} = \sum_{\vec{R}'} (k_\parallel - k_\perp)(\vec{\delta u}_{\vec{R},\vec{R}'} \cdot \vec{\Delta}_{\vec{R}\vec{R}'}) \cdot \vec{\Delta}_{\vec{R}\vec{R}'} + k_\perp \vec{\delta u}_{\vec{R},\vec{R}'} + a p_{\vec{R}\vec{R}'} \hat{\Delta}_{\vec{R}\vec{R}'} \tag{32}$$

Here $\vec{\Delta}_{\vec{R},\vec{R}'} \equiv \vec{u}^0_{\vec{R}'} - \vec{u}^0_{\vec{R}}$ is the vector difference between neighbors of the undistorted lattice and $\vec{\delta u}_{\vec{R},\vec{R}'} \equiv \vec{u}_{\vec{R}'} - \vec{u}_{\vec{R}} - \Delta_{\vec{R},\vec{R}'}$ is the relative displacement of the two mass points from their original locations. The model has both longitudinal ($k_\parallel$) and shear ($k_\perp$) spring constants. On the square lattice, for propagation along a symmetry axis, if the mass of the interacting mass points is m,

$$c_l^2 = \frac{k_\parallel a^2}{m}; \quad c_t^2 = \frac{k_\perp a^2}{m}. \tag{33}$$

There are two possible dynamical laws for the mass points. One is weakly damped Newtonian mechanics. With sound speeds on the order of $\sqrt{Y/\rho} \sim \sqrt{5 \times 10^7} \sim 7000$ m/s and a spatial grid on the order of $a = 1$ m this means time steps on the order of 10^{-4} s. In any given time step, all mass point coordinates controlled by elasticity are updated through a

Verlet algorithm[16]. The second possibility is to introduce damped dynamics so that particles evolve according to

$$\vec{F}_{\vec{R}} = -\gamma \dot{u}_{\vec{R}}. \tag{34}$$

If the oscillatory motions of mass points are not of interest (and we cannot see why they should be) then the damped dynamics that slave mass points to the channel seem advantageous so long as they are rapid enough so that masses can move to keep up with cracks. We have used

$$\gamma \approx 0.1\sqrt{k_{\|} m} \sim 10^6 \text{kg/s}. \tag{35}$$

We call this model pseudo-three-dimensional for the following reason. The model is posed completely in two dimensions. However, our physical picture is that whenever a crack opens up and creates a water channel $w_{ij}^{x,y}$, the model is representing the width across the minor axis of an elliptical fracture of the sort depicted in Figure 3. This picture has consequences both for the force law between mass points and for the computations for water transport.

When the distance between two mass points reaches the critical value of δ, the bond between them snaps. However, in the PKN model, this means that an elliptical crack opens up. There is still a restoring force between the mass points, but the spring constant, according to Eq. (6), is reduced by a factor of $a/(2H)$ in comparison with its value before breaking.

In particular, we identify $a^2 Y/(a(1-\nu^2))$ with the spring constant $k_{\|}$. The reason for the leading factor of a^2 is that Eq. (6) describes a pressure, and we multiply by the element area a^2 to obtain a force. After breaking, the pressure becomes $Y/(2H(1-\nu^2))$ and the force becomes $a^2 Y/(2H(1-\nu^2))$. Thus the force in Eq. (32) should be understood to mean that once bonds have broken, the forces are computed with spring constants reduced by $a/(2H)$. In particular, in the simulations, we maintained an array marking every bond as broken or unbroken. As soon as the distance between mass points passes a critical value, we set the marker to "broken" and thereafter multiply the force between the mass points by the factor of $a/(2H)$.

In addition, once the bond between two mass points breaks, the distance between the two mass points is controlled by the fluid in between them, in accord with (3). In the first time step where the bond breaks, a channel width variable $w_{ij}^{x,y}$ associated with the pair of particles whose bond has broken is set to the distance between them. To conserve fluid, the width of the neighboring channel element is reduced by the same value; there must always be precisely one such neighbor. From then on, the width of the channel is controlled by fluid motion. The pressure, as we have said, is given by the average normal force of mass points on either side. Note that since the displacement between the mass points is fixed to the value $w_{ij}^{x,y}$, the unbroken springs connecting them to adjacent mass points are in general compressed. This compressive force divided by the area a^2 of the mass element gives the pressure in the fluid.

Note that fluid in channels turns corners without difficulty, so the particular direction from which fluid is coming should not be important. This leads to the following scheme. Each channel segment interacts with (up to) six other channel segments. In the following discussion, move from using indices ij to locate channels, and use just one index l. Also drop the superscripts x,y on w. If l is the index for a segment under consideration and l' is the index of a neighboring channel, horizontal or vertical, consider the literal implementation of Eq. (3).

$$v_{ll'} = \frac{w_>^2}{12\mu}\frac{p_{l'} - p_l}{a}, \tag{36}$$

where

$$w_> = w_{l'} \text{ if } p_{l'} > p_l, \text{ else } w_l. \tag{37}$$

However, Eq. (36) is not quite right. In the PKN model, the width w_c is the minor axis of an ellipse of height H. Therefore, the total volume of fluid V contained in the crack assembly is

$$V = \sum_l \pi \left(\frac{H}{2}\right)\left(\frac{w_l}{2}\right) a. \tag{38}$$

For the simulation to correspond to a situation where water is pumped in from outside, it is necessary to add some volume of water per time, Q_l to some segments; this can be accomplished by adding a flux to the segments by

$$\pi \left(\frac{H}{2}\right)\frac{1}{2}\frac{dw}{dt} a = Q_l. \tag{39}$$

When fluid flows within a channel, the volume of fluid passing through per time in the continuum theory is (for fluid moving in the x direction) given by Eq. (5). Therefore, looking at some small segment,

$$\pi \frac{H}{4}\frac{dw_l}{dt} a = \pi \left(\frac{w_>}{2}\right)^3 \frac{H}{2}\frac{1}{4\mu}\frac{p_{l'} - p_l}{a} \tag{40}$$

Thus, the change in width of a segment is given by the net flux of water through

$$\frac{dw_l}{dt} = \frac{1}{a}\sum_{l'} v_{ll'} w_> \tag{41}$$

$$\text{with } v_{ll'} = \frac{w_>^2}{16\mu}\frac{p_{l'} - p_l}{a}. \tag{42}$$

In a closed system with no water coming in or out, which could be guaranteed by having w_l equal to zero along an outer boundary, the anti-symmetry of Eq. (42) guarantees that the sum over the volume of water $(\pi H a/4)\sum_l w_l$ remains constant in time. Thus, to summarize the features of the model that make it particular to a simulation of PKN:

1. When bonds break, rather than falling to zero, the strength of the bond drops by a factor of $a/2H$. This mimics the restoring force of the elastic medium at the top and bottom of the crack. With this addition to the model, the outer boundaries should be regions of zero pressure; otherwise restoring forces from the boundary interfere with the PKN mechanism.

2. When adding fluid at rate per time Q_0 use Eq. (39) to adjust the width of the injection element at each time step.

3. For the equation of motion of channel widths, use the velocity expression in Eq. (42), not Eq. (36). This expression accounts for the fact that fluid flows more quickly in the center of the ellipse where it is widest than at the top and bottom where it is narrow.

A few more implementation details:

1. At the moment a bond breaks and a segment fills with fluid, set the width of the channel to equal precisely the extra distance between the masses, so that transition to the new equation of motion for the masses does not result in a sudden displacement. In order to conserve fluid, subtract the fluid in this new channel from the neighboring channel. Although this is not an event whose magnitude drops to zero as the time step vanishes, it does not appear to cause any sort of instability.

2. After the bond between two mass points breaks and it fills with fluid, it is the distance w_c between them that is determined by the evolution equations. This prescription does not however completely specify their location. The correct position must be chosen to minimize the local elastic energy, or equivalently, to have equal forces acting from each side. We found a simple algorithm that lets us achieve this condition by having particles naturally relax towards it, rather than taking time at each step to compute the energy minimum for particles on either side of the channel. The procedure should be exact in the limit of small time steps. Here is how it works. At every time step we let particles on either side of the channel move as if the fluid was not present and exerts no force on them. Channel boundary particles under greater pressure from the rock move farther in this step. Next we compute the center of the two channel elements and move them outward about it so as to obtain the correct channel width.

3. In order to compute the pressure, the mass points on either side of a channel must have springs pushing on them. This would not be true if we allowed both springs on opposite sides of a mass point to break, and the pressure would be indeterminate. Therefore, once the spring on one side of a mass point has broken, we declare the one on the opposite side unbreakable.

Simulation Test Cases

Figure 6 shows a comparison of theory and numerical experiment for a geometry in which a single crack nucleates and runs. The simulation region is 5 m wide along x and 200 m tall along y with flexible boundaries. A horizontal seed crack 5 m wide is placed in the 3 m from the bottom of the system, and a vertical seed crack 1 m tall is placed just above it. The system is set to be 10 m in thick in the z direction. Water is injected at the spot indicated with a dot

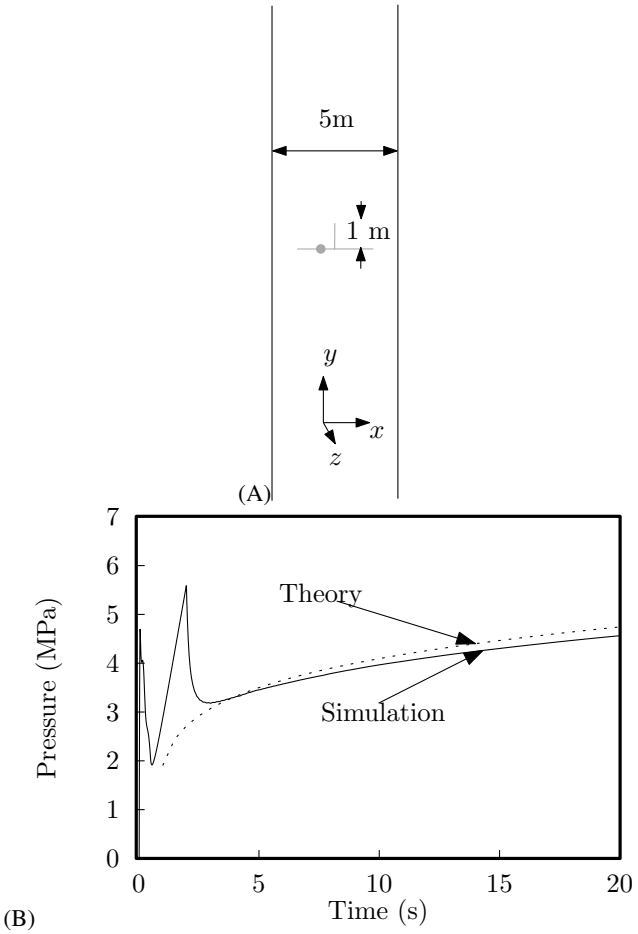

Figure 6: (A) Crack geometry. There is initially a horizontal channel and a vertical seed crack 1m high. The system is 5 m wide with stress-free boundaries. The dot indicates the fluid injection point. (B) Pressure versus time, theory and simulation. The simulation was carried out with $H = 10$ m, $Q = 18.5$ bbl/min, $Y/(1-\nu^2) = 50$ GPa.

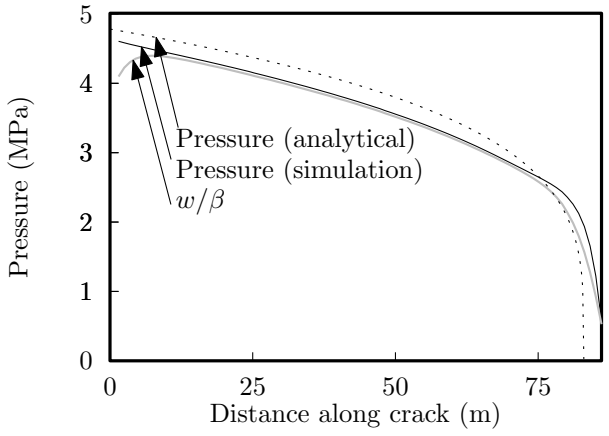

Figure 7: Comparison of simulation results for pressure with the analytical expression Eq. (7), and also a test of the relation between P and w given in Eq. (6).

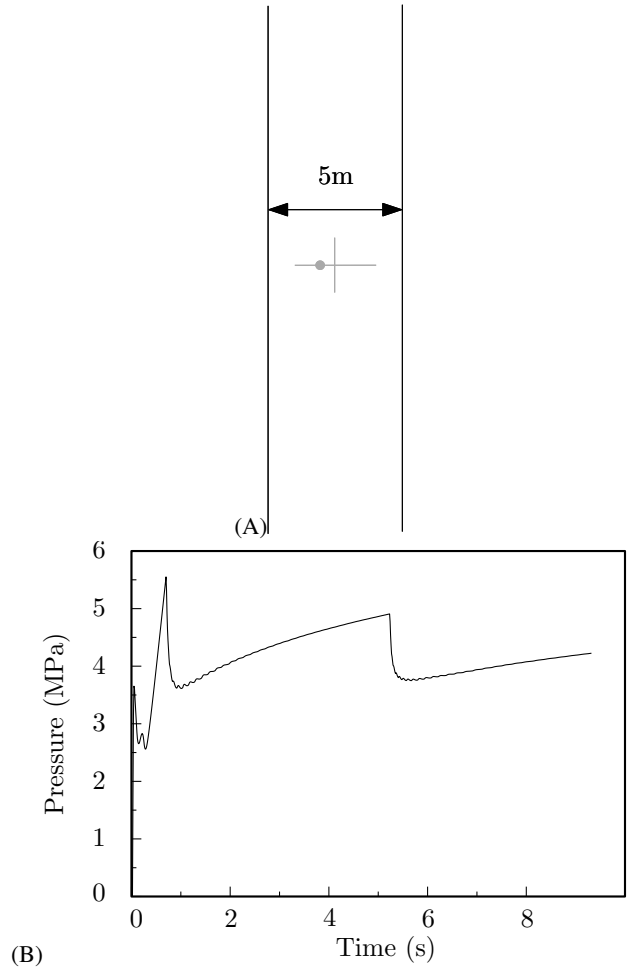

Figure 8: (A) Configuration with two seed cracks, each 1 m long, on opposing sides of a well. The dot shows the location of water injection (B) Pressure versus time showing pressure drops corresponding to initiation of the two cracks.

at 18.75 bbl/min. Comparison with numerics is computed from Eq. (17) with $\tilde{Q} = 3/8$, $\tilde{H} = 1/3$, $\tilde{Y} = (1-\nu^2)$, which gives $P = 2.63(\tilde{t}-.5)^{1/5}$MPa, since the crack initiates at 0.5 s. Pressure at the base of the crack in the simulation agrees reasonably well with the prediction of Eq. (17). According to Eq. (19) at 20 s the crack should be 83 m long. In the simulation at this time it is 85 m long.

The pressure at initiation is higher than calculated from continuum arguments. According to Eq. (27), a 1 m seed crack should initiate at a pressure of 1.6 MPa. In Appendix A we show that very short cracks in the lattice are not predicted well by continuum expressions. For a seed crack one lattice spacing long, the lattice prediction is that the crack should initiate at 5.64 MPa. The system in Figure 8(B) initiates at 5.58 MPa, in reasonable agreement with the lattice prediction.

Two additional qualitative phenomena were noted during the simulations. The first is shielding, also known as stress shadowing. If two seed cracks are pointed in the same direction, the first one to start imposes compressive stress on the base of the second and suppresses it. Explicit, approximate analytical expressions for this effect were obtained by Geilikman and Wong [17]. If the pressure at the base of the crack is P, then nearby the compressive stress is also P. More generally, if at perpendicular distance d from a long crack there is a second crack of length L and height H, then the second crack instead of experiencing an opening pressure P will experience the (net) pressure

$$P\left(1+\frac{1}{(d/H)^2+(d/L)^2}\right)^{-3/2}. \qquad (43)$$

To assess the significance of this effect, we carried out a series of simulations where a long growing crack was placed at distance d from a crack of initial length $L_0 = 2$ m. Combining Eqs. (17) and (43), the second crack should initiate when the pressure reaches some fixed critical value, and this happens at a time t from initiation of the first crack given by

$$t/t_\infty = \left(1+(L_0/d)^2\right)^6. \qquad (44)$$

Here t_∞ is the initiation time in the limit that the separation between the cracks d becomes large; the height $H = 10$ m can be neglected because it is sufficiently larger than L_0.

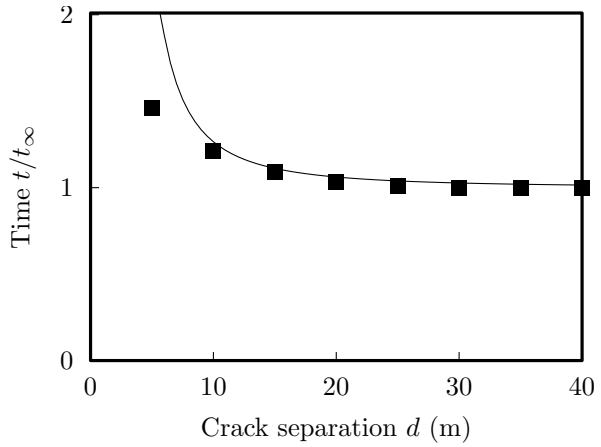

Figure 9: Two cracks are placed at perpendicular distance d from each other. The leftmost one begins to grow. If the rightmost one were very far away it would begin to grow at time t_∞, but because of shielding from the left it takes longer. The solid line shows the estimate Eq. (44) for L_0 =2m. The solid squares show results of numerical simulations.

While in general outline Eq. (44) is correct, it does not capture the numerical results with much accuracy, as shown in Figure 9. At a distance of 5 m from a large main crack, the time to initiation is predicted to increase by a factor of 3, but in the numerics increases by only 50%. From this and other numerical explorations, we find that the analytical expression for shielding overstates the effect at short distances. Note furthermore that at a distance of 15 m the shielding effect is negligible. Thus shielding may be less important in practice than it seems at first. We should, however, acknowledge that the numerical model itself has limitations that we will discuss in the closing section.

The second phenomenon is ballooning. A long crack opens up like a balloon and can absorb a lot of water if the

water is injected slowly enough. That this is possible follows from the fact that in the limit where injection rate Q becomes small, the pressure at the base of advancing cracks in Eq. (17) vanishes as $Q^{1/4}$, while the minimum pressure needed to break rock is given by Eq. (27). This pressure drops as one over the square root of crack length. Thus there exists an injection rate small enough to allow a first crack to grow to any desired length before triggering a second.

This makes it difficult to initiate any other cracks. Thus a thought about a qualitative strategy: use rapid pressure pulses. Once seed cracks get started, it is much easier for them to continue to run.

Systematic Variation of Parameters

The numerical model can be used for the systematic variation of factors that can affect the total area of a hydrofractured network. Here we provide an example in which we fix the system size, pumping rate, pumping time, and vary external stress anisotropy and its angle relative to the well. Stress anisotropy is well known to affect well completion [17–19]. If relative to the background lithostatic stress there is compression along some direction then the stress will suppress cracks from growing in that direction and either stop them or cause them to turn. For this reason, it is generally favorable for a horizontal well to be perpendicular to the direction of maximum horizontal stress, $\Sigma_{\rm max}$. In this way cracks coming out of the horizontal well are parallel to the compressive stress, which does not force them closed.

We examined this phenomenon in a series of simulations. The system is $250 \times 20 \times 10$ m, with the 10 meter height treated with the pseudo-three-dimensional method of this section. Starting with an initial condition with four seed cracks of two meters in length placed horizontally in the center of the system, we injected water in the center for two minutes at 37.5 barrels/minute (= 0.1 m^3/s). The resulting crack pattern is illustrated in Figure 10. When the compressive stress is in the horizontal direction, long cracks grow in each direction away from the seed, with ten parallel cracks forming in the end. When the compressive stress is at 45 degrees to the horizontal direction, the cracks form a complex network, tending to run parallel to the maximum compressive stress until they hit the boundaries of the system. When the compressive stress is in the vertical direction, four long cracks form in the end, and the injected water causes them to expand like balloons without further growth or triggering additional cracks.

The findings from a systematic collection of runs varying the magnitude of the stress anisotropy and its direction are summarized in Figure 11. In the previous section we found that seed cracks of order one to two meters begin to run when the pressure reaches a value of around 4 MPa. Here we find that external compressive stress anisotropy of this magnitude is able to substantially suppress the growth of a fracture network, with the greatest effects occurring when the direction of the stress is parallel to the well, and tending to close cracks coming from it.

IV. CONCLUSIONS

We begin this paper by indicating a reason to believe that hydrofractured wells with economically viable production must result from fracture networks with spacing on the order of a meter. We then develop analytical and numerical results that may assist in the understanding of how this happens.

We assemble results from the PKN model of hydrofracture and provide a number of results which although elementary we have not found assembled in one place, such as the total energy dissipated in viscous flow, the pressure at which a first fracture initiates, and the pressure at which a second fracture initiates when the first is already running. We note that because of viscous dissipation, the pressure at the base of a running hydrofracture will eventually become large enough to trigger a second one in the vicinity of the well.

Through a simple extrapolation of our analytical results to multiple cracks, we show that given the quantity of water injected into fracture stages, and typical dimensions of the fractured regions, we obtain a characteristic spacing of the fracture network based on the physics of fracture that is comparable to the spacing indicated earlier by production data.

It is natural to ask if the characteristic one-meter spacing we previously obtained from analysis of production data, and here obtain from a completely separate set of arguments having to do with mechanics of fracturing finds verification from additional sources. In sandstones, Hooker et al. [20] have presented a universal law of cumulative fracture frequency versus aperture and predict clusters of macrofractures spaced by 1 m up to 10 m. According to [21], all rock on the Earth breaks in a self-similar fashion, and a comparable frequency of natural fracture clusters would be expected in mudrocks.

We last propose a numerical model in which fluid modeled with the lubrication approximation interacts with a discrete model of an ideally brittle solid. This leads to a hydrofracture simulation in which the number and direction of hydrofractures is not specified in advance. We check this numerical model against a number of analytical calculations, and then demonstrate its use in a systematic investigation of the effects of stress anisotropy. We find, as expected, that it is favorable to drill horizontal wells perpendicular to the maximum compressive stress.

We highlight some of the advantages and disadvantages of this numerical approach. The advantages include the ability to simulate a dynamical interacting rock-water-fracture system on the scale of hundreds of meters, and the ability to allow the system to choose crack paths rather than select them in advance. There are also disadvantages. The spatial resolution of the numerical grid is coarse; each point represents cubic meters of rock. Therefore the representation of matter displacement fields is coarse. The numerical representation of continuum mechanics is stable, but cannot be expected to be precise, particularly on scales less than a meter. Furthermore, cracks are constrained to jump one meter at a time, and are only allowed to choose between horizontal and vertical motion in any given jump. As shown in Figure 10, by jumping back and forth between horizontal and vertical segments, the crack can eventually follow a path at

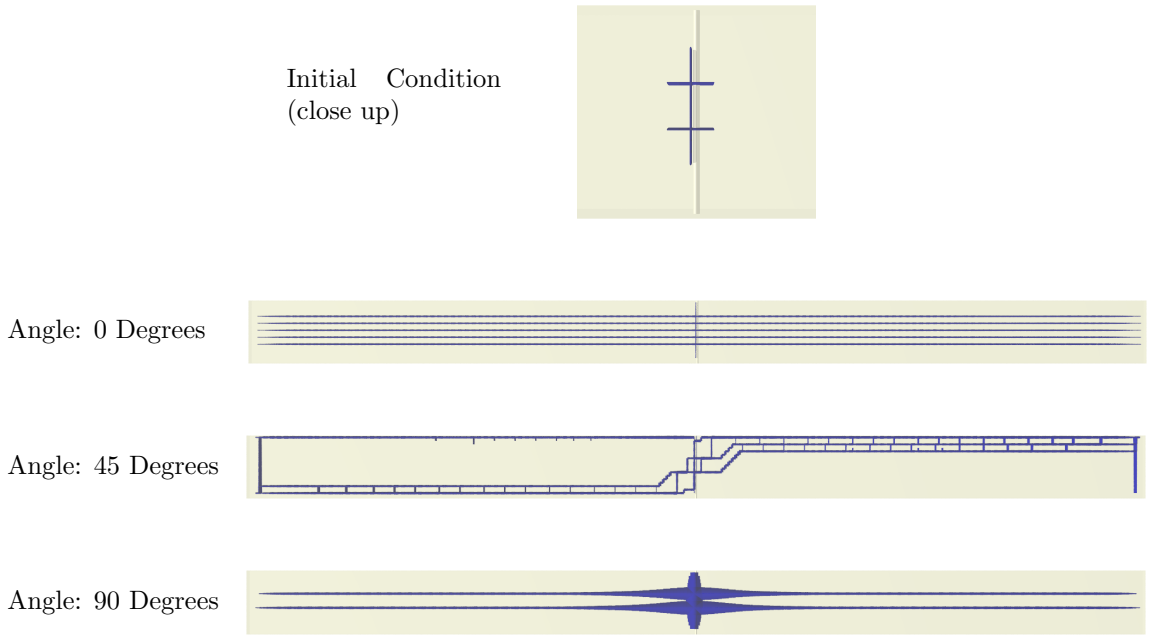

Figure 10: (Color online) Fracture network created by two minutes of pumping water at the rate of 37.5 barrels per minute into a region of size 250×20 m. Blue regions are cracks filled with water. The vertical tube represents an intial long crack into which water is injected at one point. The initial condition also has two horizontal seed cracks of four meters in length, centered on the vertical crack. A net compressive stress of 10 MPa has been applied at three different angles in relation to the horizontal axis.

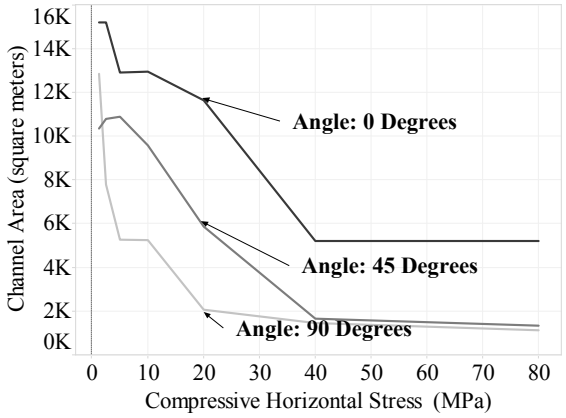

Figure 11: Total area of channel network created by systematic variation of the magnitude and angle of stress anisotropy in hydraulic fracture simulation. The area is given by multiplying the total length of the channels (in meters) by a height of 10 meters. The fractures are created by pumping 37.5 barrels per minute for two minutes.

any angle, but the bias towards moving along two particular directions is strong. The fracture toughness of shale is highly anisotropic (see for example the photograph of the Utica Shale in [22]), but the model is unlikely to capture the effect accurately without further experimental input. Finally, the real experimental setting is fully three-dimensional, allowing cracks to advance in ways that cannot be captured in our pseudo-three-dimensional formulation. For this reason a fully three-dimensional version of the code is being developed.

Nevertheless, the results in this paper contribute to the knowledge base that may allow improvement of the hydrofracturing process. The differences of production from nearby wells with seeming identical geophysical parameters can be large. When production is poor, it is not generally clear whether the fractures generated by the completion process were unfavorable, or whether there is a local deficit of hydrocarbons. An improved understanding of the physical process by which fluid-driven fractures create fracture networks may be able to assist.

Acknowledgments

This paper was supported by the Shell UT project "Physics of Hydrocarbon Recovery" with Patzek and Marder as co-PIs. MM acknowledges partial support from the National Science Foundation Condensed Matter and Materials Theory program.

[1] D. L. Turcotte, E. Moores, and J. Rundle, Physics Today **67**, 34 (2014).

[2] S. Dunn, *Fracking 101: Breaking down the most important part of today's oil, gas drilling*, The Tribune, Greely and Weld County, Colorado (January 5, 2014), URL `http://bit.ly/GreelyFracking`.

[3] T. Patzek, F. Male, and M. Marder, PNAS **110**, 19731 (2013).

[4] T. K. Perkins and L. R. Kern, Journal of Petroleum Technology pp. 937–949 (1961).

[5] R. P. Nordgren, Society of Petroleum Engineers Journal **12**, 306 (1972).

[6] R. Clifton, A. Abou-Sayed, and C. Brechtel, Journal of Geophysical Research **83**, 2851 (1978).

[7] R. Clifton, E. Simonson, and A. Abou-Sayed, Society of Petroleum Engineers Journal **8**, 27 (1978).

[8] R. Clifton, in *Advances in Hydraulics Fracturing*, edited by J. L. Gidley (SPE, 1989).

[9] R. Clifton, Q. Guo, and J. Wang, Journal of Applied Mechanics **63**, 287 (1996).

[10] M. Wangen, Computational Geosciences **17**, 647 (2012).

[11] J. Adachi, E. Siebrits, A. Peirce, and A. J. Desroches, International Journal of Rock Mechanics & Mining Sciences **44**, 739 (2007).

[12] H. Lamb, *Hydrodynamics* (Cambridge University Press, 1895), URL `https://openlibrary.org/books/OL7133467M/Hydrodynamics`.

[13] I. N. Sneddon and H. A. Elliott, Quarterly of Applied Mathematics **4**, 262 (1946).

[14] J. Fineberg and M. Marder, Physics Reports **313**, 1 (1999).

[15] J. Q. Norris, D. L. Turcotte, and J. B. Rundle, Phys. Rev. E **89**, 022119 (2014), URL `http://link.aps.org/doi/10.1103/PhysRevE.89.022119`.

[16] L. Verlet, Phys. Rev. **159**, 98 (1967).

[17] M. Geilikman and S.-W. Wong (2013), pp. SPE 167161/1–13.

[18] A. P. Bunger, X. Zhang, and R. G. Jeffrey (2012), pp. SPE 140426–PA/1–15.

[19] T. Beard, *EPA hydraulic fracturing workshop* (March 10- 11, 2011), URL `http://bit.ly/EPAHF2011`.

[20] J. N. Hooker, S. E. Laubach, and R. Marrett, Geological Society of America Bulletin **126**, 1340 (2014).

[21] M. A. Sadovskiy, Doklady Akademii Nauk SSSR **247**, 829 (1979).

[22] *Utica shale* (Retrieved December 2015), URL `https://en.wikipedia.org/wiki/Utica_Shale#/media/File:Joints_1.jpg`.

[23] P. F. Walsh, Engineering Fracture Mechanics **4**, 533 (1972).

Appendix A: Fracture properties of lattice model

The force rule in our lattice is that when two neighboring particles move away from their original locations, they exert a force on each other proportional to the change in displacement $\vec{\delta}$. When the original displacement in the lattice between the particles $\vec{\Delta}$ is parallel to $\vec{\delta}$, the force constant is $k_{\|}$ and when the original displacement is perpendicular, the force constant is $k_{\perp}$. This choice provides both longitudinal and shear waves. However, it produces a highly orthotropic solid, with $C_{14} = 0$. Although in most cases orthotropic solids have fracture properties indistinguishable from isotropic solids, in special cases the stress intensity factor can differ by a factor of up to three[23]. Very short cracks in our lattice provide one of those cases.

To check carefully, consider a square lattice of unit spacing as described above in which at sites (0,1) and (1,1) there is a positive force p and a corresponding negative force p at (0,0) and (1,0). Then the displacement of all particles in the lattice is given by

$$u_{\vec{R}} = \frac{p}{(2\pi)^2}\int_0^{2\pi} dk_x \int_0^{2\pi} dk_y \frac{e^{-i\vec{k}\cdot\vec{R}}\left(e^{ik_y}-1\right)\left(e^{ik_x}+1\right)}{k_{\|}\left(e^{ik_y}-1\right)\left(e^{-ik_y}-1\right)+k_{\perp}\left(e^{ik_x}-1\right)\left(e^{-ik_x}-1\right)} \tag{A1}$$

From this computation, one deduces that if the vertical bonds above (0,0) and (1,0) are broken, then the force p_c that would have to be applied in order to raise the bond between (2,1) and (2,0) to the breaking point δ_c is

$$p_c = \frac{p\delta_c}{2u_{(2,1)}}\left(1 - 2u_{(1,1)}\frac{k_{\|}}{p}\right). \tag{A2}$$

Carrying out this computation with a fast Fourier transform, one finds a result that for an edge crack a of length one lattice spacing translates to

$$p_c = 1.79\sqrt{\frac{\Gamma Y}{a(1-\nu^2)}} \tag{A3}$$

However, the isotropic continuum result is

$$p_c = .504\sqrt{\frac{\Gamma Y}{a(1-\nu^2)}}. \tag{A4}$$

Thus the discrete orthotropic lattice requires a pressure more than three times higher to fracture an edge crack than predicted by the continuum.